https://doi.org/10.30799/jnst.239.19050209 J. Nanosci. Tech. - Volume 5 Issue 2 (2019) 682–687

Share Your Innovations through JACS Directory

Journal of Nanoscience and Technology

Visit Journal at http://www.jacsdirectory.com/jnst

ISSN: 2455-0191

Study on Structural and Optical Properties of Ni and Mn Codoped TiO_2 Nanomaterials and Its Application in Visible Light Photocatalytic Activity of Indigo Caramine Dye

Sankara Rao Miditana, T. Siva Rao*, Shaik Abdul Alim

Department of Inorganic & Analytical Chemistry, A.U. College of Science & Technology, Andhra University, Visakhapatnam – 530003, Andhra Pradesh, India.

ARTICLE DETAILS

Article history:
Received 20 April 2019
Accepted 06 May 2019
Available online 16 May 2019

Keywords:
Ni-Mn Codoped TiO_2
Indigo Caramine
Photocatalysis
Sol-Gel Synthesis

ABSTRACT

To enhance the photocatalytic activity of TiO_2 in visible light, nickel and manganese codoped TiO_2 (NMTs) and undoped TiO_2 nanomaterials were synthesized by varying dopant concentrations using a solgel method. As prepared nano materials were characterized by using X-ray diffraction (XRD) and its results shows anatase and rutile mixed phase was observed for codoped catalyst samples. Rough morphology, irregular particle shape and elemental composition of catalyst were identified with scanning electron microscopy (SEM) and energy dispersive X-ray spectroscopy (EDX) respectively. The Fourier transform infrared spectroscopy (FT-IR) result revealed that the substitutional doping of Mn^{2+} and Ni^{2+} into TiO_2 lattice by replacing Ti^{4+} in TiO_2 lattice. This was confirmed by shifting of stretching frequencies of Ti-O-Ti from 569 cm^{-1} – 608 cm^{-1}. The catalyst (NMT2) exhibits least band gap (2.7 eV), less particle size (6.5 nm) with high surface area (135.70 m^2/g) when compared to undoped TiO_2 (3.2 ev, 18.3 nm, 64.09 m^2/g), which were determined by UV-visible diffused reflectance spectroscopy (UV Vis-DRS), transmission electron microscopy (TEM) and Brunauer-Emmett-Teller (BET) respectively. Based on the characterization results the efficiency of codoped catalyst were exhibits better photocatalytic degradation of indigo caramine (IC). The results show that IC has degraded within 90 minutes at doping concentrations 1.0 wt% of Ni^{2+} ion and 0.25 wt% of Mn^{2+} ion in TiO_2 (NMT2) at an optimum reaction parameter pH-3, catalyst dosage 0.080 g/L and at IC dye concentration of 0.020 g/L.

1. Introduction

In the present-day scenario, most of the textile industrial discharges contains cosmogenic azo dyes having appreciable concentrations of materials with high chemical oxygen demand and suspended solids may posing adverse effects to both human and aquatic life. Moreover, the washed dyes colours released into the effluent interfere with the transmission of sun light into water bodies. This in turn inhibits the photosynthesis activity of aquatic biota besides direct toxic effects on biota. Indigo Carmine (IC), a blue synthetic dye, is used in textile industry for dyeing of fabrics [1,2]. Heterogeneous photocatalytic oxidation using semiconductors is an effective technique for air and water decontamination. TiO_2 is generally accepted as one of the most effective photo-induced catalysts and is frequently used to oxidize organic and inorganic compounds in air and water due to its strong oxidative ability and long-term photo-stability. TiO_2 is also a very common, non-expensive and non-toxic material [3]. It exists in three crystalline structures; anatase, rutile and brookite. Anatase and rutile belong to the large bandgap semiconductors with bandgap energies of 3.2 and 3.0 eV, respectively [3]. Anatase is basically the polymorph phase which has widely been used in photo-catalytic processes for de-pollution purposes. However, it has been indicated that combination of anatase and rutile are photo-catalytically more active than pure anatase or pure rutile phases of TiO_2 separately [4].

To address this problem many researchers attempted the doping of metal ions [5] an optimum concentration of the dopants favoured to control the crystallite size of nano metal doped TiO_2, decrease in bandgap and facilitate the formation of high specific surface area [6]. According to literature survey many reports illustrated that the doping of transition metal such as Mn and Ni [7] into TiO_2 lattice causes distortion of crystal structure and electronic structure due to interaction of d- orbitals of doped transition metal ions with Ti-3d orbital below the conduction band and reduce the band gap and electronic transition energies [8]. Moreover, transition metals can also suppress the e-/h+ recombination during irradiation. The metal doped TiO_2 was obtained by dissemination of metal nano particles, into TiO_2 matrix. An appended benefit of transition metal doping like Mn, Cr, Ni, Cu [9,10] were improved the trapping of electron to inhibit the e^+/h^- recombination during irradiation of light.

In the present investigation, among all the transition metals manganese and nickel were selected for the synthesis of Mn-Ni codoped TiO_2 by using solgel method. These metals are preferred because the presence of t_{2g} orbital of d is very close to conduction band by which the absorption shifted to visible region [8,11]. Manganese has the greatest potential in permitting significant optical absorption in the visible region, through the combined effects of narrow bandgap and the introduction of intermediate bands within forbidden gap [8]. In the Mn-Ni codoped TiO_2 Mn^{2+} and Ni^{2+} ions are easily replacing the Ti^{4+} in TiO_2 lattice because ionic radii of Ti^{4+} (0.068 nm) is similar with ionic radii's of Mn^{2+} (0.078 nm) and Ni^{2+} (0.072 nm) [12]. On other hand, the introduction of Ni ions in TiO_2 lattice can form heterojunctions between n-type TiO_2 and p-type Ni oxide dopant. The presence of p-n junctions can promote the separation of electron-hole pairs through the electric junction field and facilitate the interfacial charge transfer [13].

The synthesized samples were tested for its photocatalytic efficiency using a model pollutant indigo caramine. One of the most widely used dyes in the textile industry is IC or acid blue 74, which is also used as an additive in pharmaceutical tablets and capsules and for medical diagnostic purposes [1]. However, IC dye causes irritation to the gastrointestinal tract leading to vomiting and diarrhea. It may also cause irritation to the respiratory tract. Symptoms may include coughing and shortness of breath. IC containing effluents are generated from textiles, printing, cosmetics and plastic industries, etc., [14].

2. Experimental Methods

2.1 Materials

All the chemicals used in the synthesis process were reagent grade and used without further purification. N-butyl tetra ortho titanate ($Ti(OBu)_4$), manganese nitrate $[Mn(NO_3)_2].6H_2O$ and nickel nitrate $[Ni(NO_3)_2].6H_2O$ were obtained from E-Merck Germany and used as a precursors for

*Corresponding Author:sivaraoau@gmail.com(T. Siva Rao)

https://doi.org/10.30799/jnst.239.19050209

Cite this Article as: Sankara Rao Miditana, T. Siva Rao, Shaik Abdul Alim, Study on structural and optical properties of Ni and Mn codoped TiO_2 nanomaterials and its application in visible light photocatalytic activity of indigo caramine dye, J. Nanosci. Tech. 5(2) (2019) 682–687.

titanium, manganese and nickel for preparing undoped TiO_2 and co-doped TiO_2 catalysts respectively. Indigo carmine dye was used as a model dye pollutant procured from High Media, India.

2.2 Synthesis of Nano Catalyst

Manganese and nickel co-doped nano titania were synthesized by sol-gel method [15,16]. In this process n-Butyl ortho titanate (20 mL) was added to 40 mL of ethanol and acidified with 3.2 mL of nitric acid taken in a 150 mL pyrex glass beaker (solution-A) and stirred for 15 min. In another beaker required weight as per the dopant weight percentage of Mn and Ni from its precursors with respect to titania weight percentage were taken and added 40 mL of ethanol and then 7.2 mL of deionised water for the purpose of hydrolysis process (solution-B). Then solution- B was added to solution-A drop wise under vigorous stirring. After complete addition of solution (B), a colloidal suspension formed and continues stirring for 90 min and kept for aging for 48 h. The obtained gel was dried in an oven at 70 °C and grounded in motor and pestle and calcined at 450 °C for about 5 h in a muffle furnace. Finally, it was cooled and ground to form homogeneous powder. For preparation of undoped TiO_2 was followed without addition of nickel and manganese precursors. Following the above procedure different Mn and Ni co-doped catalysts were prepared by varying weight percentages of Mn and Ni (0.25 wt.% - 1.0 wt.%) as shown in Table 1.

Table 1 Name assigned to different weight percentages of codoped TiO_2 catalyst samples

S.No.	Dopant (Transition metal) weight percentages in TiO_2(Wt%)	Name assigned to codoped TiO_2 catalyst
1	1.00 Mn 0.25 Ni	NMT1
2	0.25 Mn 1.00 Ni	NMT2
3	0.50 Mn 0.50 Ni	NMT3
4	0.25 Mn 0.75 Ni	NMT4
5	0.75 Mn 0.25 Ni	NMT5
6	Nil	undoped TiO_2

2.3 Experimental Techniques Used for Characterization of the Catalysts

The crystalline structure of photocatalysts were determined by powder X-ray diffraction (XRD) spectra taken (PAN Analytical) using anode Cu-WL 1 (λ=1.5406 nm) radiation with a nickel filter. The applied current and voltage were 40 mA and 40 kV respectively. The average crystallite size of anatase was determined according to the Scherrer equation using full width at half maximum (FWHM) data of the selected peak. X-ray photo electron spectroscopy (XPS) was recorded with a PH1 quantum ESCA microprobe system using the AlKα line of a 250W X-ray tube as a radiation source with the energy of 1253.6 eV, 16 mA x 12.5 kV and a working pressure lower than $1X10^{-8}$ Nm^{-2}. The fitting of XPS curves was analyzed with multipack 6.0 A software. The surface area and porosity measurements were carried out with a micrometrics Gemini VII surface area analyzer. The nitrogen adsorption/desorption isotherms were recorded 2-3 times to obtain reproducible results and reported by BJH surface/volume meso pore analysis. The micro pore volume was calculated using the Frenkel-Halsey-Hill isotherm equation. Each sample was degassed at 300 °C for 2 h. The size and shape of the catalyst were recorded with TEM using JEOL/JEM 2100, operated at 200 kV. The morphology and elemental composition of the catalyst were characterized using scanning electron microscope (SEM) (ZEISS-SUPRA 55 VP) equipped with an energy dispersive X-ray (EDS) spectrophotometer and operated at 20 kV. FT-IR spectra of the samples were recorded on a FT-IR spectrometer (Nicolet Avatar 360). The Diffuse reflectance spectra (DRS) of the catalyst samples were recorded with a Shimadzu 3600 UV-Visible-DRS Spectrophotometer equipped with an integrating sphere diffuse reflectance accessory, using $BaSO_4$ as reference scatter. Powder samples were loaded into a quartz cell and spectra were recorded in the range of 200-900 nm. The extent of IC degradation was monitored using UV-Vis spectrophotometer (Shimadzu 1601).

2.4 Determination of Photo Catalytic Activity of the Catalyst

The photocatalytic efficiency of the synthesized catalyst, Mn and Ni codoped nanotitania was determined by degradation of IC dye under visible light irradiation in the photocatalytic reactor [17]. A high pressure 400 W (35,000 lm) mercury vapour lamp with UV filter (Oriel, 51472) was used as a visible light source. The degradation procedure was performed by taking 100 mL of dye solution of required concentration (1-10 mg/L) containing sufficient amount of the catalyst in a 150 mL Pyrex glass vessel under continuous stirring placed about 20 cm away from the light source. The running water was circulated around the sample container to filter IR radiation and also to maintain constant solution temperature in the reaction. Before irradiation of the solution was stirred in dark for 30 min to attain adsorption – desorption equilibrium of IC dye on the catalyst surface. After visible light illumination 5 mL of aliquots samples were collected from the reaction mixture using millipore syringe (0.45 μm) at different intervals of time to observe the change in IC dye concentration by measuring the absorbance at 609 nm using UV-visible Spectrophotometer. A pH meter (Elico Digital pH meter model 111E, EI) was used for adjusting and investigation of pH variation during the degradation process. The pH of the dye solutions was adjusted prior to illumination and during the degradation process by addition of 0.1 N NaOH / 0.1 N HCl to get required pH. The percent of degradation of IC dye was calculated from the following equation [16],

$$\% \text{ of Degradation} = A_0 - A_t / A_0 \times 100$$

where, A_0 is initial absorbance of dye solution before degradation and A_t is absorbance of dye solution at time t. The optimum reaction conditions are attained by varying the reaction parameters, such as effect of dopant concentration, effect of pH, catalyst dosage and initial dye concentration.

3. Results and Discussion

3.1 XRD Study

Fig. 1 shows crystallinity, specific surface area, and structural properties of manganese and nickel codoped TiO_2 of different phases in the XRD patterns of the samples obtained after calcinations at 450 °C. All diffraction lines are relatively strong, which indicating a high crystallinity for all samples. Further, the peak positions and relative intensities of the diffraction lines match with standard diffraction data for different TiO_2 phases, i.e. anatase and rutile NMT1 –NMT2, NMT3. The anatase phase was confirmed with the Joint Committee on Powder Diffraction Standard (JCPDS) file no. 21-1272. The peaks at 2θ= 25.28, 37.81 and 48.05° corresponded to the (101), (004), and (200) planes of anatase. While the peaks at 2θ= 27.29, 44.10 and 54.32, corresponded to the (110), (101) and (220) planes of rutile structure with the JCPDS file no. 21-1276 [18]. The existence of rutile in the nanomaterial was readily discernible from its (110) diffraction peak located at 2theta of 27.29° in the XRD pattern, because no overlapping of this peak with any other peaks from anatase occurred. Anatase phase can be also easily identified from its (101) peak located at 2theta of 25.3°, as this peak doesn't overlap with any other peaks of rutile. This result clearly demonstrates that rutile and anatase coexisted in the samples NMT1-NMT3. Further the samples NMT4 –NMT5 and undoped TiO_2 shows anatase phase only. The X-ray diffraction patterns of anatase TiO_2 nanoparticles exhibited broad peaks, indicating small sizes of the nanoparticles at 450 °C calcination temperature while the sharp peaks indicated large sizes of the nanoparticles. The average crystallite sizes of the samples were determined by calculating the Debye–Scherrer equation by using high intensity of anatase (101) and rutile (110) diffraction peaks, the results were shown in Table 3. The XRD patterns of the samples exhibited similar diffraction peaks, indicating that the obtained samples were the TiO_2 nano material consisting of anatase and rutile nanoparticles.

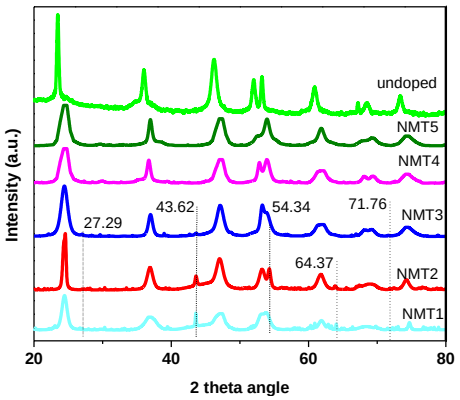

Fig. 1 XRD patterns of undoped and codoped NMTs catalysts

3.2 Scanning Electron Microscopy

The morphology and particle size of the catalyst play very important role in its photocatalytic activity [15] and were examined by the SEM. Fig. 2 shows that the SEM micrograph of the as prepared undoped and codoped NMT2 TiO_2 Nanoparticles. In the Fig. 2(a) undoped TiO_2 clearly revealed large particle size and Fig. 2(b) codoped TiO_2 shows small particle size, which leads to high surface area it correlates with BET results. The morphology has different shapes of grains with irregular

https://doi.org/10.30799/jnst.239.19050209

boundaries. Images of undoped TiO_2 (Fig. 2(a)) show randomly shaped and aggregated particles. HRSEM of 1.00 wt.% of Ni and 0.25 wt.% of Mn–TiO_2 (Fig. 2(b)) shows irregular tiny clusters composed of large numbers of nanoparticles with lower aggregation and better distribution. From the SEM images it can be inferred that aggregation is decreased greatly due to co-doping. The elemental composition of the prepared catalyst determined by the EDS detector was attached to a SEM shown in Fig. 2c. EDX analysis revealed that the presence of Ti, O, Ni and Mn elements.

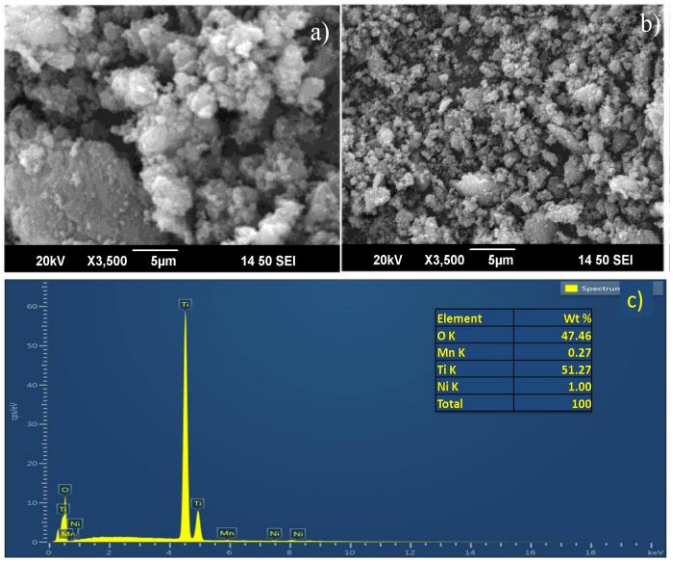

Fig. 2 SEM images a) undoped TiO_2 b) NMT2 codoped TiO_2 and c) NMT2 codoped TiO_2 EDX spectra

3.3 Transmitted Electron Microscopy Study

The particle size distribution was obtained by measuring the diameter of particles from representative TEM images. The TEM micrographs of undoped and codoped (NMT2) TiO_2 samples are shown in Figs. 3(a) and (b). From the images it is noticed that the particle size of NMT2 is smaller size compared to undoped TiO_2. The Fig. 3c shows the catalyst particles lattice fringes with d spacing 0.33 nm corresponding to 101 planes of anatase phase of TiO_2. The diffraction rings are observed (Fig. 3d) for co-doped (NMT2) TiO_2 catalyst from SAED pattern is clearly reveals that no structural change of anatase TiO_2 was found, the planes are (101), (004), (200) and (211). Fig. 3(e) shows that the average size of the prepared nano particle is 6.5 nm, which was calculate from Gaussian fitting of the size histogram [19,20]. These results confirmed that the co-doping of Ni and Mn reduces the particle size of TiO_2.

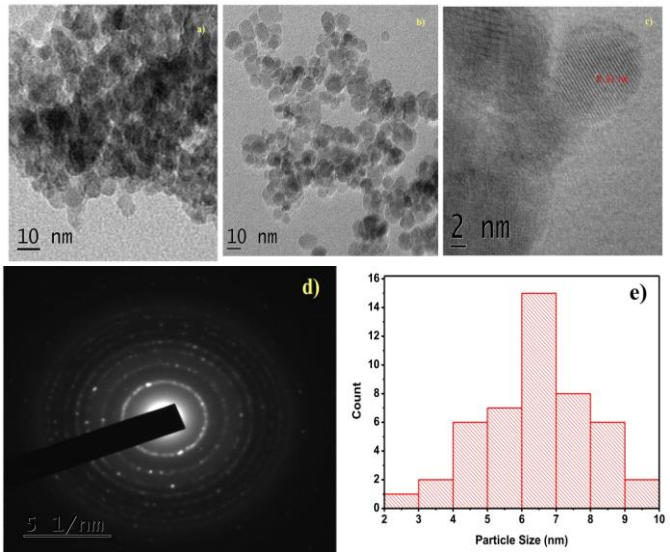

Fig. 3 TEM images a) undoped TiO_2 b) NMT2 codoped TiO_2 c) NMT2 codoped TiO_2 lattice fringes, d) SAED pattern of NMT2 and e) NMT particle size distribution

3.4 FTIR Characterization

Undoped and Ni^{2+}, Mn^{2+} codoped TiO_2 nano materials were identified by FT-IR spectra and were given in Fig. 4. The peaks appeared around at 3012 cm^{-1}- 3464 cm^{-1}, 1620 cm^{-1} – 1635 cm^{-1} [21] corresponding to stretching vibrations of OH belongs to Ti-OH on the surface and bending vibrations of adsorbed H-OH molecule. The strong absorption band around 569 cm^{-1} is due to stretching vibrations of Ti-O-Ti and Ti-O band in undoped TiO_2 which is in good agreement with previous studies [22]. From Fig. 4a it is seen that after codoping of Ni and Mn into TiO_2 lattice the stretching vibrations of skeletal Ti-O-Ti shifted to 569 cm^{-1} – 605 cm^{-1} indicated that Ni and Mn codoped in to TiO_2 lattice by substituting titanium [23]. Further, there is appearance of the band located at 1020 cm^{-1} for codoped TiO_2 indeed that Ni and Mn codoped into TiO_2 lattice.

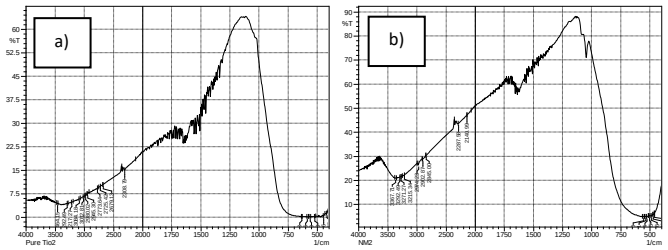

Fig. 4 FTIR spectra of a) undoped TiO_2 b) NMT2

3.5 UV DRS Study

The diffused reflectance spectra (DRS) of undoped and Ni,Mn codoped TiO_2 samples were given in Fig. 5 indicate that the absorption of the electromagnetic spectrum appeared at the visible region at about (400 nm–800 nm). NMTs (Ni and Mn) codoped samples shows remarkable decreases in band gap and extension of absorption edge towards visible light wave length (red shift). This is may be due to the formation of an extra energy level above the valance band by Ni 2p narrowing the band gap of TiO_2 [24].

This shift is associated with the doping as well as the formation of stable rutile phase of TiO_2 as illustrated in XRD. The inherent reason for red shift in the band gap is due to the change of the sp-d exchange interactions between the band electrons and the localized d-electrons of the Ni^{2+} ions [25].

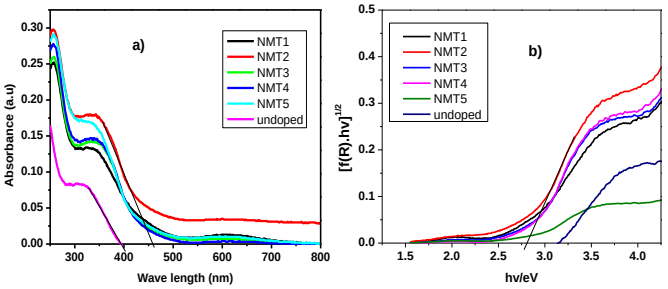

Fig. 5 (a) The DRS spectra of undoped and codoped TiO_2 with different weight % of Mn and Ni; (b) Tauc plots of the square root of the Kubelka-Munk function determining band gap energy values

The manganese ion incorporated into TiO_2 lattice and it distorts the surrounding environment which effects the conduction band through the interaction with Ti-3d orbital's which facilitate the suppresses the recombination of electron hole pairs extended the optical response energy [26]. Further it was supported by the calculated band gap energies of all the synthesized samples from the reflectance spectra using the Kubelka-Monk formalism and Tauc plot method [27] shown in Fig. 5(b). The undoped TiO_2 exhibited the band gap of 3.2 eV which is comparable with the literature value [28] and the codoped TiO_2 sample showing the band gap ranging from 2.7 to 3.01 eV. Among all the codoped samples NMT2 exhibiting less band gap energy (2.70 eV). Thus, the results indicated that all the codoped samples are visible light active and enhances the photocatalytic degradation efficiency due to formation of a greater number of photo generated electron/hole pairs. Further, when compared the band gap values of Mn and Ni single doped TiO_2 catalysts (which are obtained from literature value) the band gap of NMT2 catalyst is reduced and the values are given in Table 2 [29,30].

Table 2 The comparative band gap values of Mn and Ni single doped and Mn and Ni codoped TiO2

S.No.	Doping elements	Catalysts Band gap energy (eV)	Reference
1	Mn	2.95	[28]
2	Ni	2.99	[29]
3	Undoped TiO_2	3.2	[27]
4	Mn and Ni	2.70	Present work

https://doi.org/10.30799/jnst.239.19050209

Cite this Article as: Sankara Rao Miditana, T. Siva Rao, Shaik Abdul Alim, Study on structural and optical properties of Ni and Mn codoped TiO_2 nanomaterials and its application in visible light photocatalytic activity of indigo caramine dye, J. Nanosci. Tech. 5(2) (2019) 682–687.

3.6 Brauner-Emmett-Teller (BET)

The specific surface area and porosity of the mesoporous TiO_2 were investigated by using the N_2 adsorption and desorption isotherms before and after the calcination as shown in Fig. 6a. All the isotherms of samples reveal the stepwise adsorption and desorption branch of type IV curves, indicating the presence of mesoporous material having a three-dimensional (3D) intersection according to the IUPAC classification. A hysteresis loop with a stepwise adsorption and desorption branch is observed at wide range of pressure (P/Po), and the surface area of NMT2 mesoporous TiO_2 calcined at 450 °C is 135.70 m^2/g as shown in Fig. 6a. The undoped TiO_2 surface area is 64 m^2/g as shown in Fig. 6a. This result indicates that the synthesized material has wider mesoporous structure. To analysis pore size and pore volume, the plots of the pore size distribution are investigated by desorption branch of the BJH method as shown in Fig. 6b. The average pore diameter of mesoporous TiO_2 calcined at 450 °C is 6.2 nm with relatively narrow pore size distribution. The pore volume of mesoporous TiO_2 is 0.22 cm^3/g. However, undoped TiO_2 10 nm pore size distribution is observed and 0.21 cm^3/g pore volume is also counted. Such a physical properties of large surface area and high crystallinity with nanocrystalline aggregated is good candidate material for high photocatalytic activity. This is may be attributed that increased surface area favours the adsorption of the greater number of dye molecules on the surface of the catalyst and it enhances the degradation efficiency of the catalyst.

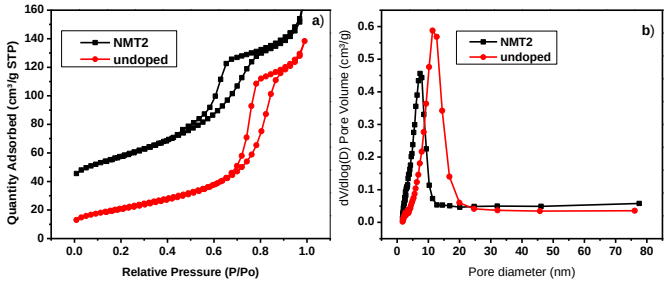

Fig. 6 (a) The N_2 adsorption–desorption isotherms and (b) pore diameter distribution curves of NMT2 codoped TiO_2

Table 3 The Results of crystallite size (XRD), Band gap (UV-Vis- DRS) and BET surface area

S.No.	Catalyst code no	Crystallite size (nm)	Band gap Energy (eV)	BET surface area analysis		
				Surface area (m^2/g)	Pore Volume (Cm^3/g)	Pore Size (nm)
1	NMT1	7.35	2.74	113.41	0.22	7.3
2	NMT2	6.5	2.70	135.70	0.22	6.2
3	NMT3	7.31	2.78	114.06	0.22	7.3
4	NMT4	7.9	2.84	106.81	0.20	8.2
5	NMT5	8.50	3.0	88.87	0.20	9.3
6	undoped	18.3	3.20	64.09	0.21	10

3.7 Assessment of Photocatalytic Efficiency

To establish an optimum reaction parameter for efficient photocatalytic degradation of IC dye with NMT2 catalyst the experiments were carried out under visible light irradiation. The rate of degradation of dye was measuring its absorbance (at λ max - 610 nm) during the reaction at different intervals of time. Before proceeds for above process, the reactions are conducted to understand interdependency of the light, catalyst and dye. The first instance a fixed amount of dye solution was taken in a beaker and stirred for the solution 60 min in dark and exposed to visible light. In both the solution there is no decrease in the absorbance of the dye was observed. This indicated that only the visible light cannot degrade the dye. In the second instance both catalyst and dye were taken in a beaker and stirred for 60 min in dark and exposed to visible light. In dark condition slight decreases in the absorbance was noticed. These observations illustrated that in the dark reaction there is an adsorption of dye molecules on the surface of the catalyst was taken place. Hence, little decrease in the absorbance of dye was observed for the solution. In visible light these adsorbed molecules are gets degraded due to activation of the catalyst particles by expose of visible light. Hence, there is a drastic decrease in the absorbance of dye solution. This indicated that to get the degradation of the dye, light and catalyst are important factors to achieve complete degradation of the dye not only these two parameters (catalyst, Dye) but other parameters such as dopant concentration, pH of the solution, catalyst dosage and initial dye concentration are the required parameters to optimize these parameters, experiments were carried out for the degradation of IC dye by varying one of these parameters and other parameters kept constant.

3.7.1 Effect of Dopant Concentration

The effect of dopant concentration of undoped and Ni, Mn codoped TiO_2 nano catalysts were studied for photocatalytic efficiency for degradation of indigo caramine at 10 mg/L, catalyst dosage 0.070 g/L and pH-4. The experiments results were drawn in Fig. 7. From the figure all the codoped samples shows better photocatalytic activity than that of undoped TiO_2 in visible light. But, NMT2 showed highest photocatalytic activity compared to other codoped samples. This is may be attributed that all the NMTs samples shows anatase and rutile phase with reduced bandgap and small particle size, which helps the highest rate of photo degradation of Indigo Caramine. Among all the codoped catalysts NMT2 having less band gap, it absorbs a greater number of visible light radiation by the catalyst particles and produces more e^-/h^+ which assist the high rate of degradation of IC.

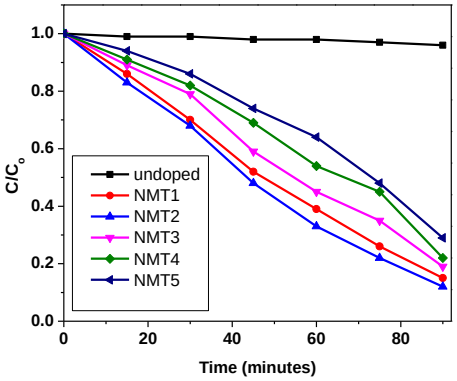

Fig. 7 Effect of dopant concentration on photocatalytic of codoped titania for rate of degradation of IC dye. Here, catalyst dosage 0.070 g/L, pH-4 and IC= 10 mg/L

3.7.2 Effect of pH

Solution pH is an important variable parameter in the evaluation of photocatalytic dye degradation efficiency of the catalyst in aqueous medium. In order to explore the effect of pH on the catalyst surface dark reactions were conducted without pH and with pH at 3, 4, 7 and 10. 5 mL of aliquots were collected every 10 min during the stirring and absorbance of dye solution was measured at 610 nm. Fig. 8a illustrates that the negligible adsorption was observed without pH, the curve observed is parallel to X-axis. From Fig. 8a at pH-3 the rate of adsorption of dye molecules were increased up to 24 min and later it become constant, this indicates that the dye molecules are adsorbed on the surface of the catalyst in a single layer, after that the adsorption may not take place. Hence, the curve becomes constant. At pH-3 the adsorption of dye molecules is very high. From Fig. 8a at pH-5 the adsorption decreases compared to pH-3 and no adsorption was observed at pH-10. At pH-3 the rate of adsorption is very high because in this dark reaction the addition of the solution order was changed as follows, catalyst solution was taken into the beaker and pH was adjusted by addition of 0.1 M HCl and stirred the solution for 15 min and the dye solution was added.

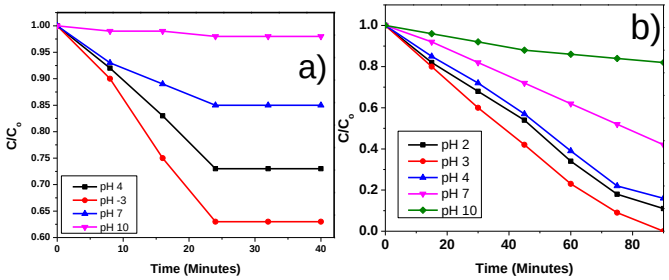

Fig. 8 a) Effect of pH in dark condition on the adsorption of IC dye, NMT2 Catalyst dosage 0.080 g/L, dye 20 mg/L b)The effect of catalyst dosage on the degradation of IC dye NMT2 catalyst, pH-3 and dye 20 mg/L

Due to the addition of the HCl solution in this order before addition of the dye solution to the catalyst surface becomes positive, which is ready for the electrostatic interaction with negative dye molecule [31]. The adsorption is very high at pH-3 up to 24 min. The effect of pH on the percentage of degradation of IC was studied by varying the pH from pH-2 to pH-10 as the adsorption of the dye on the catalyst surface is depends on the pH [32] and other parameters kept constant at catalyst dosage 0.080 g/L and initial dye concentration 10 mg/L with NMT2 catalyst. The experimental results presented in Fig. 8b indicated that at pH-3 the rate of degradation of IC was maximum. The rate of degradation of dye has to be interpreted in terms of electrostatic interaction between catalyst surface and substrate (dye) molecules. This is may be interpreted that if may

https://doi.org/10.30799/jnst.239.19050209

increasing the metal ion dopant concentration in the TiO_2 lattice the surface of the catalyst becomes more +ve due to formation of M-OH (M-OH= Ti-OH or Mn-OH) groups. At pH-3 more H^+ ions are available which can attacks the OH groups of the M-OH groups and make the surface of the catalyst more +ve [33].

$TiOH + H^+ \rightarrow TiOH_2$ pH < 6.25

$TiOH \rightarrow TiO^- + H^+$ pH > 6.25

The presence of OH groups on the surface of the catalyst can be characterized by FT-IR OH stretching frequencies. Once the surface of the catalyst becomes +ve (at pH-3) the –ve dye molecules are electro statically interacted with +ve surface of the catalyst [34] and facilitate the reaction between OH radical, which produces at surface of the catalyst and adsorbed dye molecules. Hence, the rate of degradation increases.

3.7.3 Effect of Catalyst Dosage

A most appropriate catalyst concentration must be determined in order to avoid the catalyst wastage and provide the total absorption of photons. Hence, to obtain optimum catalyst dosage experiments were performed by changing the NMT2 catalyst concentration from 0.020 mg/L to 0.1 mg/L at fixed pH-3 and IC dye concentration 20 mg/L. From Fig. 9 the optimum catalyst dosage was found to be 0.080 mg/L which shows higher rate of degradation. At < 0.080 mg/L of catalyst dosage a moderate rate of degradation was observed due to a smaller number of catalyst particles are available for a greater number of dyes molecules. Further at > 0.080 mg/L of catalyst dosage the rate decreases even though a greater number of catalyst particles are available. This may be attributed that the catalyst dosage increases the turbidity of the solution, which retards the penetration of the light and limits the activation of the catalyst particles [35]. Hence, the rate of degradation decreases.

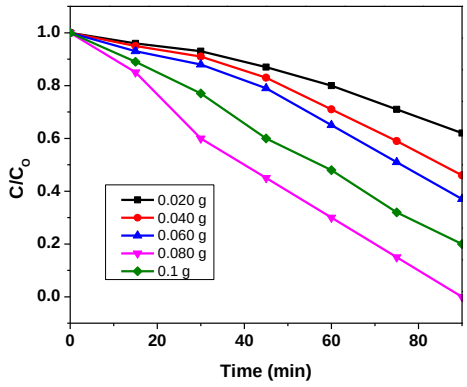

Fig. 9 Effect of NMT2 catalyst dosage, pH-3 and IC concentration 20 mg/L

3.7.4 Effect of Initial Dye Concentration

To study the effect of initial concentration of IC dye at a fixed weight of NMT2 catalyst dosage (0.080 mg/L) and at pH-3, the experiments were carried out with different concentrations of IC dye from 5 ppm to 25 ppm and results are presented in Fig. 10. These Results indicated that the rate of degradation of IC dye increased up to 20 ppm later decreases [36]. This can be explained by correlating with TEM and BET characterization results. The decreased particle size (6.5 nm) and high surface area (135.70 m^2/g) the rate of dye molecules adsorbed on the surface of the catalyst increases which favours the close proximity with the •OH. It facilitates the reaction between •OH and substrate molecules and leads to high rate of degradation of IC dye.

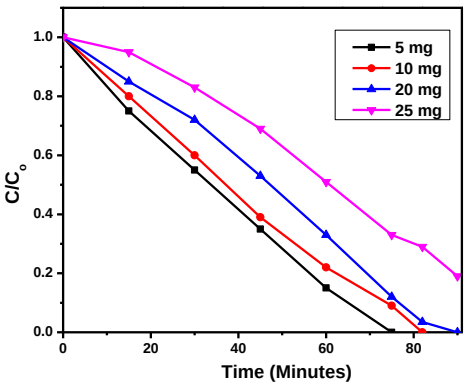

Fig. 10 IC initial concentration at pH-3, NMT2 catalyst concentration 0.080 g/L

4. Conclusion

In the present work we have successfully synthesized Ni^{2+} and Mn^{2+} co-doped TiO_2 (NMTs) nano catalysts were prepared by solgel method. All the codoped TiO_2 nano catalysts shows better photocatalytic activity than undoped TiO_2, it is experimentally proved. From the FTIR spectroscopic technique it is confirmed that Ni^{2+} and Mn^{2+} are incorporated into the TiO_2 lattice. Due to the incorporation of Ni^{2+} and Mn^{2+} into TiO_2 lattice the experimental results reveals that codoped catalysts (NMTs) shows smaller in size, larger in surface area and having less band gap values which are confirmed by XRD, BET, UV–vis DRS instrumental techniques respectively. Among all the codoped catalysts NMT2 (1.0 wt% Ni^{2+} and 0.25 wt% Mn^{2+}) codoped TiO_2 nano catalyst was shows higher photocatalytic activity. This brings to form more electron capture traps, which provides high separation efficiency of photo generated carriers. Finally, the 1.0 wt% Ni^{2+} and 0.25 wt% Mn^{2+}codoped TiO_2 exhibiting the high photocatalytic activity for the degradation of 20 mgL^{-1} IC at pH-3 with 0.080 g/L catalyst weight.

References

[1] R. Uma Lakshmi, Vimal Chandra Srivastava, Indra Deo Mall, Dilip H. Lataye, Rice husk ash as an effective adsorbent: Evaluation of adsorptive characteristics for Indigo Carmine dye, J. Environ. Manag. 90 (2009) 710-720.
[2] Y. Anjaneyulu, N. Sreedhara Chary, D. Samuel Suman Raj, Decolourization of industrial effluents – available methods and emerging technologies – a review, Environ. Sci. Biotechnol. 4 (2005) 245–273.
[3] V. Binas, D. Venieri, D. Kotzias, G. Kiriakidis, Modified TiO_2 based photocatalysts for improved air and health quality, J. Mater. 3 (2017) 3-16.
[4] S.S. Muniandy, N.H. Mohd Kaus, B. Zhong Tao Jiang, C. Mohammednoor Altarawnehc, H. Ling Lee, Green synthesis of mesoporous anatase TiO_2 nanoparticles and their photocatalytic activities, RSC Adv. 7 (2017) 48083-48090.
[5] V.D. Binas, K. Sambani, T. Maggos, A. Katsanaki, G. Kiriakidis, Synthesis and photocatalytic activity of Mn-doped TiO_2 nanostructured powders under UV and visible light, Appl. Catal. B: Environ. 113–114 (2012) 79-86.
[6] N.T. Yong, L.W. Chung., R.M. Abdul, An overview on the photocatalytic activity of nano-doped-TiO_2 in the degradation of Organic Pollutants, ISRN Mater. Sci. 2011 (2011) 1-18.
[7] S. Noor Begum, H.M. Farveez Ahmed, K. R. Gunashekar, Effects of Ni doping on photocatalytic activity of TiO_2 thin films prepared by liquid phase deposition technique, B. Mater. Sci. 31(2008) 747–751.
[8] Y. Fei Zhao, L. Can, L. Song, R. Xi Liu, J. Yuan Hu, Y. Yan Gong, L. Yuan Niu, Electronic, optical and photocatalytic behavior of Mn, N doped and codoped TiO_2: Experiment and simulation, J. Solid State Chem. 235 (2016) 160–168.
[9] K. Umar Azmi Aris, H. Ahmad, T. Parveen, J. Jaafar, Z. Abdul Majid, et al., Synthesis of visible light active doped TiO_2 for the degradation of organic pollutants-methylene blue and glyphosate, J. Anal. Sci. Tech. 7 (2016) 20-29.
[10] D. Jing, Y. Zhang, L. Guo, Study on the synthesis of Ni doped mesoporous TiO_2 and its photocatalytic activity for hydrogen evolution in aqueous methanol solution, Chem. Phy. Lett. 415 (2005) 74-78.
[11] M. Pelaez, N.T. Nolan, Suresh C. Pillai, M. Seery, A Review on the visible light active titanium dioxide photocatalysts for environmental applications, Appl. Catal. B: Environ. 125 (2012) 331-349.
[12] C. Shifu, Z. Sujuan, L. Wei, Z. Wei, Preparation and activity evaluation of p–n junction photocatalyst NiO/TiO_2, J. Hazard. Mate. 55 (2008) 320–326.
[13] K. Wilke, H.D. Breuer, The influence of transition metal doping on the physical and photocatalytic properties of titania, Int. J. Photo Energy 121 (1999) 49–53.
[14] J.F. Porter, G. McKay, K.H. Choy, The prediction of sorption from a binary mixture of acidic dyes using single- and mixed-isotherm variants of the ideal adsorbed solute theory, Chem. Eng. Sci. 54 (1999) 5863-5885.
[15] B.K. Avasarala, T. Siva Rao, S. Bojja, Enhanced photocatalytic activity of beryllium doped titania in visible light on the degradation of methyl orange dye, Int. J. Mater. Res. 101 (2010) 1–7.
[16] S. Abdul Alim, T. Siva Rao, I. Manga Raju, M. Ravi Kumar, K.V. Divya Lakshmi, Fabrication of visible light driven nano structured Copper, Boron co-doped TiO_2 for photocatalytic removal of Lissamine Green B, J. Sau. Chem. Soc. 23 (2019) 92-103.
[17] J.C.S. Wu, C.H. Chen, A visible light responsive vanadium doped titania nanocatalyst by sol-gel method, J. Photochem. Photobiol. A: Chem. 163 (2014) 509-515.
[18] N. Wetchakun, B. Incessungvorn, K. Wetchakun, S. Phanichphant, Influence of calcination temperature on anatase to rutile phase transformation in TiO_2 nanoparticles synthesized by the modified sol–gel method, Mater. Lett. 82 (2012) 195–198.
[19] E. Gharibshahi, E. Saion, Influence of dose on particle size and optical properties of colloidal platinum nanoparticles, Int. J. Mol. Sci. 13 (2012) 14723-14741.
[20] K. Taranjeet, S. Abhishek, T. Amrit Pal, R.K. Wanchoo, Utilization of solar energy for the degradation of carbendazim and propiconazole by Fe doped TiO_2, Solar Energy 125 (2016) 65–76.
[21] Y. Zhongping, J. Fanghou, T. Shujun, C. Xiang, J. Zhaohua, B. Xuefeng, Microporous Ni-doped TiO_2 film photocatalyst by plasma electrolytic oxidation, Appl. Mater. Sci. 2 (2010) 2617-2622.
[22] N. Sharotri, D. Sud, A greener approach to synthesize visible light responsive nanoporous S-doped TiO_2 with enhanced photocatalytic activity, New J. Chem. 39 (2015) 217-223.

https://doi.org/10.30799/jnst.239.19050209

Cite this Article as: Sankara Rao Miditana, T. Siva Rao, Shaik Abdul Alim, Study on structural and optical properties of Ni and Mn codoped TiO_2 nanomaterials and its application in visible light photocatalytic activity of indigo caramine dye, J. Nanosci. Tech. 5(2) (2019) 682–687.

[23] I. Othmana, R.M. Mohamed, F.M. Ibrahem, Study of photocatalytic oxidation of indigo carmine dye on Mn-supported TiO_2, J. Photochem. Photobiol. A: Chem. 189 (2007) 80–85.
[24] S. Jensen, S. Dmitri Kilin, Electronic properties of nickel-doped TiO_2 anatase, J. Phy. Cond. Mat. 27 (2015) 1-13.
[25] S. Munir Shah, S.M.H. Hussain, Effect of carrier concentration on the optical band gap of TiO_2 nanoparticles, Mater. Des. 92 (2016) 64–72.
[26] Y. Wang, R. Zhang, Jianbao, Li. Liangliang, Li. Shiwei Lin, First principles study on transition metal-doped anatase TiO_2, Nanoscale Res. Lett. 9 (2014) 35-46.
[27] S. Chang, H. Chien-yao, L. Pin-han, T. Chang, Preparation of phosphated Zr doped TiO_2 exhibiting high photocatalytic activity through calcination of ligand-capped nanocrystals, Appl. Catal. B: Environ. 90 (2009) 233-241.
[28] D. Christian, A.M. Pérez-Osorio, S. Christopher Kley, P. Punke, E.C. Patrick, et al., TiO_2 anatase with a bandgap in the visible region, Nano Lett. 14 (2014) 6533–6538.
[29] R. Chauhan, A. Kumar, R. Pal Chaudhary, Structural and photocatalytic studies of Mn doped TiO_2 nanoparticles, Spectrochem. Acta A 98 (2012) 256-264.
[30] V. Bhatia, A. Dhir, Transition metal doped TiO_2 mediated photocatalytic degradation of anti-inflammatory drug under solar irradiations, J. Environ. Chem. Eng. 4 (2016) 1267–1273.
[31] H. Huang, R. Cao, S. Yu, K. Xu, W. Hao, et al., Single-unit-cell layer established Bi2WO6 3D hierarchical architectures: efficient adsorption, photocatalysis and dye sensitized photoelectrochemical performance, Appl. Catal. B 219 (2017) 526–537.
[32] G. Zeng, J. Wan, D. Huang, L. Hu, C. Huang, et al., Precipitation, adsorption and rhizosphere effect: the mechanisms for Phosphate-induced Pb immobilization in soils-A review, J. Hazard. Mater. 339 (2017) 354–367.
[33] K. Wang, Y. Hisieh, C. Wu, C. Chang, The pH and anion effects on the heterogeneous photocatalytic degradation of o-methyl benzoic acid in TiO_2 aqueous suspension, Chemosphere 40 (2000) 389-397.
[34] M.A. Rauf, S. Salman Ashraf, Fundamental principles and application of heterogeneous photocatalytic degradation of dyes in solution, Chem. Eng. J. 5 (2009) 10–18.
[35] N. Venkatachalam, M. Palanichamy, V. Murugesan, Sol-gel preparation and characterization of alkaline-earth metal doped nano TiO_2: efficient photocatalytic degradation of 4-chlorophenol, J. Mol. Catal. A: Chem. 273 (2007) 177–185.
[36] C.H. Chiou, R.S. Juang, Photocatalytic degradation of phenol in aqueous solutions by Pr-doped TiO_2 nanoparticles, J. Hazard. Mater. 149 (2007) 669-678.

https://doi.org/10.30799/jnst.239.19050209

Cite this Article as: Sankara Rao Miditana, T. Siva Rao, Shaik Abdul Alim, Study on structural and optical properties of Ni and Mn codoped TiO_2 nanomaterials and its application in visible light photocatalytic activity of indigo caramine dye, J. Nanosci. Tech. 5(2) (2019) 682–687.